Segmentation and Data Extraction from Carte du Ciel Astrographic Maps

Lasko M. Laskov[0000−0003−1833−8184] and Ivon Nikolova[0009−0004−2293−2121]

New Bulgarian University, Informatics Department
llaskov@nbu.bg, ivonnikolova0101@gmail.com

Abstract. The goal of our research is to develop a set of methods and algorithms for automatic data extraction from images of historical astrographic plates. We focus on scanned *astrographic maps* that are result of the 19th century huge astronomical project Carte du Ciel.
The goal of Carte du Ciel, along with Astrographic Catalogue, was to map the stars up to 14th magnitude in the entire visible sky. The result is stored in the form of photographic plates and their paper copies, called *astrographic maps*. They contain valuable information for researchers in the field of astronomy, mainly because of the age of the data, and are a subject of extensive research.
In this paper we present our approach for segmentation of images of astrographic maps and automatic extraction of the triple stars images (called asterisms) that are contained in them. The presented method creates a data set of asterisms whose purpose is to train a convolutional neural network for automatic flare stars detection in the astrographic maps.

Keywords: Image processing · Pattern recognition · Astrographic maps · Carte du Ciel.

1 Introduction

Carte du Ciel together with *Astrographic Catalogue* formed a vast international astronomical project that continued from 1887 until 1962 [6]. The goal of the project was to map the positions of the stars in the whole visible sky as faint as 11th magnitude, and to map the relative positions of the stars of 14th magnitude and brighter [15]. Twenty observatories around the world participated, collecting the resulting glass photographic plates, that are referred to as *astrographic plates* [3], which were used as well to create the catalogue of stars positions (Astrographic Catalogue), and the atlas (Carte du Ciel) [14].

The astrographic plates themselves have the following physical characteristics. The size of the plates is 16×16 cm with the area covered with photographic emulsion is 13×13 cm [14], [9]. The photographed field is $2^\circ \times 2^\circ$. When the plates were exposed, the location in the neighboring plate was selected in such way, so that its corner lies at the center of the current one, which means that one quarter of a plate overlaps with an neighboring one [6]. Each plate was exposed

three times, with each exposure with approximate duration of 15 to 30 minutes. As a result, each star is represented on the plate with three images that form the vertices of a triangle (see Fig. 1) which is called by Fresneau [3] *asterism*.

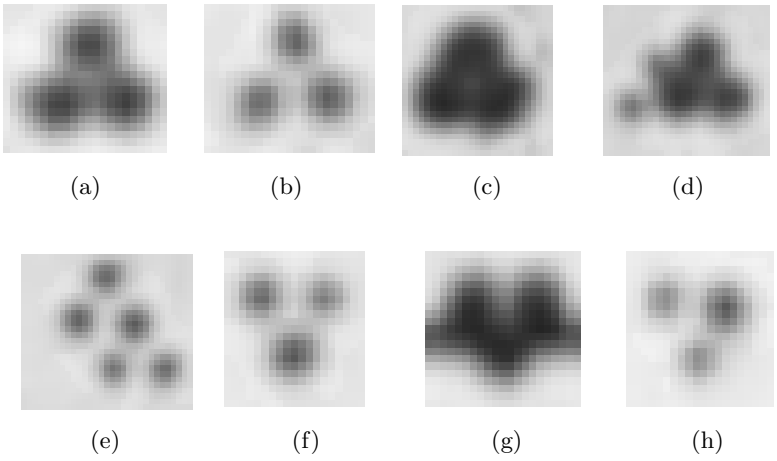

Fig. 1. Examples of triple images of a star called asterism. In some images asterisms point upwards (a) – (e), in others they point downwards (f) – (h). There are many asterisms overlapping (d), (e), or degraded by the coordinate system (g). Asterisms of stars brighter than 12th magnitude merge into a single connected component (c)

Carte du Ciel plates and Astrographic Catalogue have been a subject of extensive research in astronomy. The plates of the Royal Observatory of Belgium have been included in the digital database Wide-Field Plate Database (WFPDB) [14], and the data have been a subject of analysis by specialist in the field. Reductions of the Astrographic Catalogue using a modern reference catalog data analysis, and specialized reduction software was described in [15] where the goal was to produce a catalog of positions and proper motions in support of the Sloan Digital Sky Survey. In [11] is proposed a method for reduction of Carte du Ciel plates based on modeling of the data performed by non-linear least squares fitting of the sum of three bivariate Gaussian distributions of the asterisms. Recently, in [9] the potential of digitalization of Carte du Ciel plates with a commercial digital camera is studied. Also, in [10] the authors search for binary and multiple stars combining data of Carte du Ciel archive at the University of Helsinki and Gaia catalogue.

In [3] Fresneau investigated the potential of the Carte du Ciel plates for discovering of quick brightness changes of stars. Even though the original purpose of the triple exposure of the plates was to distinguish between the images of stars and images of other celestial bodies, such as asteroids, and to calculate the coordinates of the stars [11], the three images can contain valuable astronomical

information. A difference in the Gaussian distribution in the three star images of asterisms (see both Fig. 1f and Fig. 1h) can be an indication of an event that brings information to researchers in the field of astronomy [3], [8].

The *astrographic maps* are paper copies that are produced from the photographic plates using the technique of photogravure on copper plates. The maps are negative images in which the background is white and the stars and other light objects, are in gray scale, with brightest objects appearing black. The digital images that are subject of our research are scanned astrographic maps. The goal of this paper is to provide methods and algorithms for automatic segmentation of astrographic maps, and automatic extraction of asterisms that are contained in their images. The purpose of the presented algorithms is to extract a dataset of asterisms from digital images of astrographic maps which will be used to train and test our implementation of a convolutional neural network for asterism classification [7].

This paper is organized as follows. In Sec. 2 we describe the structure and characteristics of the Carte du Ciel digitized astrographic maps. In Sec. 3 we provide the methods for segmentation of the grid of lines on the images called *réseau*, that is used for measurement of stellar positions. Sec. 4 describes our approach for asterisms segmentation. In Sec. 5 we give brief description of our implementation and experiments results. Finally, in Sec. 4 we give conclusions and directions for future work.

2 Structure of astrographic maps

The digital images used in our research are scanned asrographic maps that are copies of the Carte du Ciel astrographic plates collected at the Royal Observatory of Belgium in Uccle. The abbreviation that denotes this dataset is ROB033 (see for details [14]). The original photographic plates are with dimensions 16×16 cm and they cover a field of $2^\circ \times 2^\circ$, taken by triple exposure. The resulting asterisms form equilateral triangle with size $11''$. The plates were enlarged twice, and then engraved on copper plates to produce their paper copies using the process of photogravure.

Digital images themselves vary slightly in dimensions between 8926×8750 pixels, 9088×8752 pixels and 9090×8752 pixels. The images are in grayscale, they are uniformly illuminated and in very good quality, which are defining characteristic for the design of segmentation algorithms.

Images are composed by top, bottom, left and right margins, and the center part that corresponds to the part of the plate covered with emulsion that contains the stellar images. The margins of the images contain various information and metadata about the plates. The top margin contains the title, the coordinates of the plate (see Fig. 2), and also zone, plate number (see Fig. 4) and the name of the observatory. Bottom margin contains the date on which the plate was exposed, and other metadata like the correspondence between the stellar images and stars magnitude (see Fig. 3).

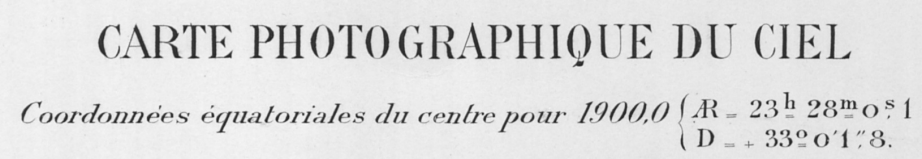

Fig. 2. Fragment from the top margin that contains title and celestial coordinates of the plate

The region of interest (ROI) for our research is the central part of the astrographic map that contains the asterisms images (see Fig. 4). It contains a square grid of straight lines that is called *réseau*. The grid is with step 5 arcmin and it was printed on the plate before its development [14], and its purpose is to measure stellar positions.

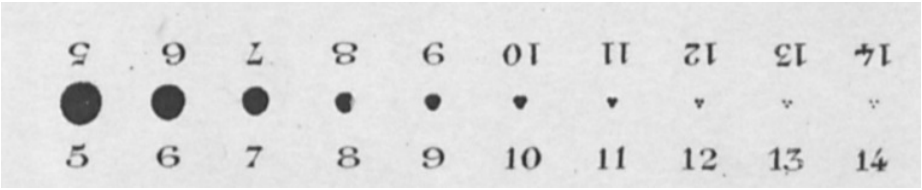

Fig. 3. Fragment from the bottom margin that contains a chart with stars images and corresponding stars magnitude

The réseau is composed by 27×27 grid of horizontal and vertical lines that form a coordinate system with its origin located in the center of the map. In both abscissa and ordinate, lines are labeled in both positive and negative directions, starting from the center line that is labeled 0 with step 5, forming the sequence of réseau labels:

$$R = \langle 60, 55, \ldots, 5, 0, 5, \ldots, 55, 60 \rangle. \tag{1}$$

The first and the last lines, both horizontal and vertical, that form the frame of the réseau are not labeled.

The réseau divides the ROI into 26×26 square regions (see Fig. 4). Each region contains asterisms, or possibly it could be an empty one, and it uniquely determines asterisms coordinates.

The images of asterisms vary from a very faint vertices forming an equilateral triangle for stars with magnitude 14 and fainter, to clearly distinguishable three stars in the same formation (13 – 11 magnitude). After stars magnitude 10 and brighter, asterisms merge into a single connected component and around magnitude 8 they appear as a single bright round image. The chart with correspondence between asterisms images and stars magnitude printed in the bottom

margin of the astrographic map unambiguously gives this correspondence (see Fig. 3).

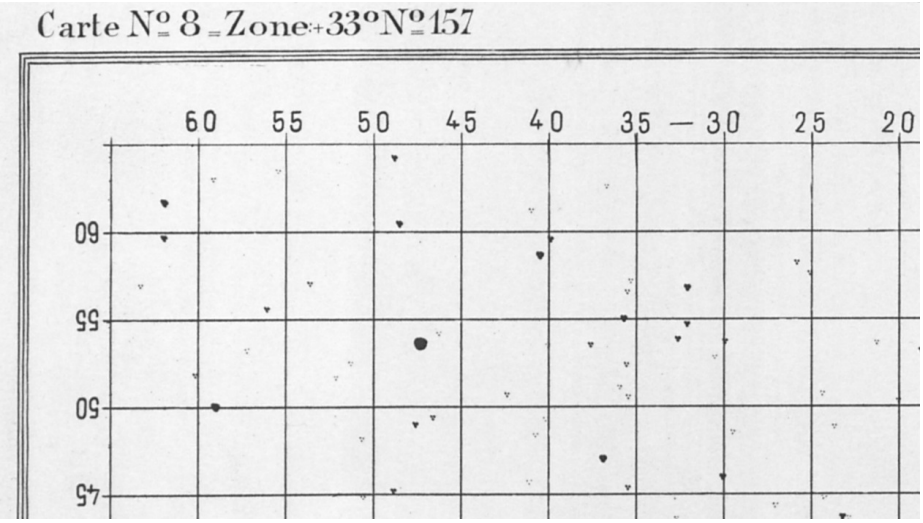

Fig. 4. Fragment that shows the upper left corner of the réseau. Part of the top margin metadata is also visible

The astrigrhic maps contain also noisy asterism images. The most common cases are:

- asterism that fall on lines of the réseau (see Fig. 1g);
- asterism whose images are overlapping (see Fig. 1d and Fig. 1e).

Since in these two cases we cannot use asterisms for data extraction, the segmentation step aims to reduce these samples.

The goal of the algorithms presented in this paper is to extract automatically those asterisms contained in the processed astrographic map, that potentially may contain data for flare stars detection [3]. This means that we are interested to extract those asterisms, that are composed by three clearly distinguishable stars images. The convolutional neural network [7] will be trained and tested using the resulting data set, and its goal is to detect those asterisms that contain a difference between the Gaussian distributions of the three stars images. Also, the design of the neural network allows the separation of those samples that correspond to noisy stars images and merged stars images. However, on the presented segmentation step we are capable of minimizing merged asterisms images in the data set.

3 Réseau segmentation

The goal of this stage of the segmentation of the astograohic maps is to extract the lines that form the réseau and to represent the input image as 26×26 square regions, which on the next stage are processed separately. The result of réseau segmentation stage allow us both to process the square regions without interfering with the printed lines of the coordinate system, and latter to use the réseau information as metadata for each asterism that corresponds to its coordinates in the astrographic plate and stars celestial coordinates.

In order to detect the lines of the réseau, first we need to segment the object pixels from the background pixels. Since we label the object pixels with the constant 1, and background pixels with constant 0 based on a selected threshold, sometimes this process in literature is referred to as *image binarization* or *image thresholding* [13].

Since the input images are of very good quality, they are uniformly illuminated, for the binariazation step we adopt the Otsu's method [12] which is a classic global threshold selection algorithm. In our implementation of the Otsu's method we follow also [4] and we are maximizing the between-class variance σ_B^2 (5) in the following steps.

Let us denote the input grayscale image with M rows and N columns with $I_{M\times N}$. With $I[i][j]$ we denote the value of the pixel located on the ith row and jth column of the image, where $i = 0, 1, \ldots, M-1$ and $j = 0, 1, \ldots N-1$.Then each pixel $I[i][j]$ is an integer value in the range $[0, L-1]$, where L is the number of intensity levels. In our case we work with $L = 256$ number intensity levels of the gray, where 0 denotes black and 255 denotes white.

As first step, we calculate the normalized histogram p of the input image I:

$$p[k] = \frac{n_k}{MN}, \text{ for } k = 0, 1, \ldots, L-1, \tag{2}$$

where n_k denotes the number of pixels in I with intensity level k. In this way $\sum_{k=0}^{L-1} p[k] = 1$, and each histogram bean $p[k]$ is an estimate of the probability of the occurrence of intensity k in I (see [4]).

The second step is to calculate the cumulative sums:

$$P[k] = \sum_{i=0}^{k} p[i], \text{ for } k = 0, 1, \ldots, L-1. \tag{3}$$

P represents the probability of occurrence of the class of the object pixels, while $1 - P$ represents the probability of occurrence of the class of the background pixels.

The third step is to calculate the class object pixels mean values

$$m[k] = \sum_{i=0}^{k} ip[i], \text{ for } k = 0, 1, \ldots, L. \tag{4}$$

Note that the global mean value m_G will be computed as the Lth component of m in (4), and thus $m_G = m[L]$.

Then, we calculate the between-class variance with:

$$\sigma_B^2[k] = \frac{(m_G P[k] - m[k])^2}{P[k](1 - P[k])}, \text{ for } k = 0, 1, \ldots, L-1. \tag{5}$$

The optimal threshold k^* is the one that maximizes σ_B^2:

$$\sigma_B^2[k^*] = \max_{1 \le k < L} \sigma_B^2[k]. \tag{6}$$

Then the binarized image $B_{M \times N}$ is calculated by globally applying the threshold k^*:

$$B[i][j] = \begin{cases} 0, & \text{if } I[i][j] \ge k^* \\ 1, & \text{if } I[i][j] < k^* \end{cases}, \tag{7}$$

for $i = 0, 1, \ldots, M-1$ and $j = 0, 1, \ldots, N-1$. Note that in the computer program implementation sometimes it is more practical to encode the background pixels with the integer value 255 and object pixels with 0.

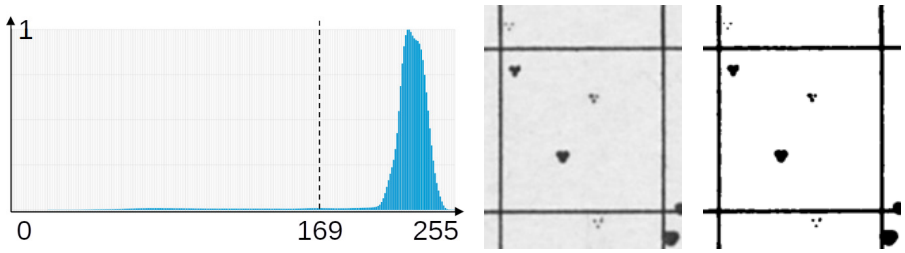

(a) (b) (c)

Fig. 5. (a) The grayscale histogram of the astrographic map ROB033 / 08 with optimal threshold found by Otsu's method $k^* = 169$; (b) fragment of the raw image; (c) fragment of the binarized image

On Fig. 5a it is given the grayscale histogram of the astrographic map ROB033 / 08. The shape of the graph shows a clearly distinguishable bimodal histogram. The Otsu's algorithm finds an optimal threshold $k^* = 169$. On Fig. 5c it is shown that the resulting binary image clearly segments the pixels of the réseau from the background pixels.

We use the binary image $B_{M \times N}$ to calculate the horizontal projective profile:

$$h[i] = \sum_{j=0}^{N-1} B[i, j], \; i = 0, 1, \ldots, M-1. \tag{8}$$

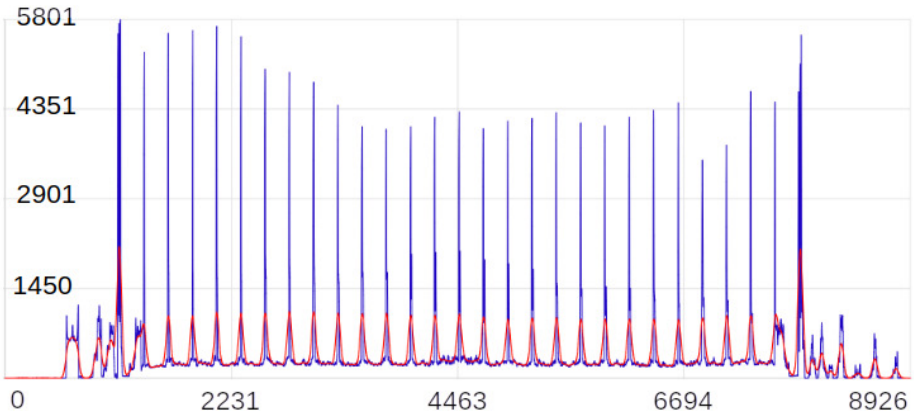

Fig. 6. The horizontal projective profile h of the binarized astrographic map ROB033 / 08 given in blue, and its smoothened version with a one-dimensional Gaussian filter in red. The abscissa represents the height of the image in pixels, and the ordinate represents the number of object pixels for the corresponding image row

The horizontal projective profile h represents a histogram that has number of beans equal to the height of the image M. Each bean corresponds to the ith row of the image and it contains the number of object pixels in it (see Fig. 6).

Analogously, we calculate the vertical projective profile of $B_{M\times N}$:

$$v[j] = \sum_{i=0}^{M-1} B[i,j],\ j = 0, 1, \ldots, N-1. \tag{9}$$

The vertical projective profile v is a histogram with number of beans equal to the width of the image N, where each bean contains the number of object pixels in the jth column of $B_{M\times N}$. The actions of the presented method with both h and v are equivalent, that is why we will illustrate them with h.

The maxima in the projective profile h correspond to the image rows that contain maximal number of object pixels. Since réseau is formed by straight, continuous lines and the scanned image is not rotated, these maxima correspond to the réseau lines locations. To extract the maxima form the projective profile, we first filter the profile with a one-dimensional Gaussian smoothing (lowpass) filter (see [4]):

$$G(r) = Ke^{-\frac{r^2}{2\sigma^2}}, \tag{10}$$

where K is a constant that substitutes the multiplier of the standard Gaussian probability density function, and σ is the standard deviation, which in our case corresponds to the number of image rows in the domain of the filter. The filtering is implemented as discrete convolution or linear spatial filtering ([4]):

$$(G \star h)[i] = \sum_{k=-m}^{m} G[k]h[i-k],\ \text{where } m = \frac{\sigma - 1}{2}, \tag{11}$$

Algorithm 1 Threshold local maxima in the projective profile

```
1: function PROFILE-THRESH(h)
2:     find indexes k1 and k2 that correspond to fames maxima
3:     a = min_{k1<i<k2} {h[i]}
4:     b = max_{k1<i<k2} {h[i]}
5:     t = (b − a)/4
6:     h̃ = (G ⋆ h)                          ▷ linear spatial filtering (11)
7:     for i = k1 to k2 do
8:         if h̃[i] < t then
9:             h̃[i] = 0
10:        end if
11:    end for
12: end function
```

for all $i = 0, 1, \ldots, M-1$.

Fig. 6 shows the original projective profile h in blue, and the filtered projective profile $(G \star h)$ (in red) with a Gaussian filter G with $\sigma = 20$. From the smoothened projective profile $(G \star h)$ we extract the maxima that correspond to the horizontal lines with a threshold technique (Alg. 1) that sets to 0 all the rest values in the array of the profile.

We apply the same filtering and threshoding algorithm on the vertical projective profile v, and we segment the vertical lines of réseau. Fig. 7 shows a fragment of the central region of the astrographic map ROB033 / 08 with the discovered réseau lines given in red color (horizontal) and blue color (vertical). The segmented réseau grid allows us to process each of the 26×26 square regions, to extract asterism from them and to store the metadata corresponding to the image and celestial coordinates of the stars represented by the corresponding asterisms.

4 Asterisms segmentation

The second stage of the presented method is the segmentation of asterisms from the scanned astrographic maps. We process each of the segmented 26×26 square regions separately and we apply a combination of Circle Hough Transform (CHT) and a clustering algorithm.

Hough Transform (HT) [5] is a classical algorithm in image processing for feature extraction even for imperfect shapes. Initially it was developed to extract straight lines in images, and after that generalization of the method was proposed to detect arbitrary geometrical shapes [1]. Since the images of the stars are Gaussian distributions of the grayscale in circular shape (see Fig. 1), we apply the generalization of the HT for circle detection CHT [16].

CHT is a voting algorithm that builds a parameter space based on the circle equation:

$$(x-a)^2 + (y-b)^2 = r^2, \tag{12}$$

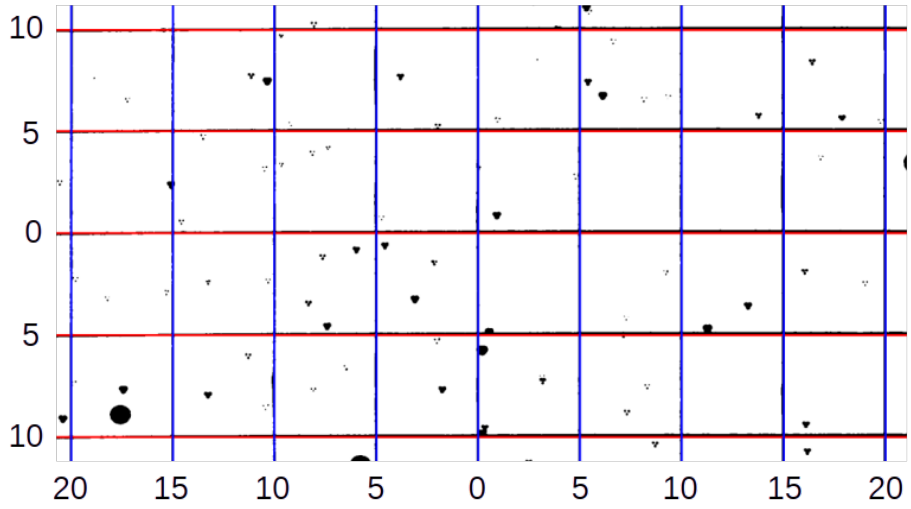

Fig. 7. Fragment of the central region of the binarized astrographic map ROB033 / 08 with segmented réseau. Horizontal réseau lines are given in red, and the vertical are given in blue

in which (a, b) represents the center of a circle, and r is its radius. For the purpose of the parameter space definition, more robustly to represent the circle equation in parametric form:

$$\begin{aligned} x &= a + r\cos\theta \\ y &= b + r\sin\theta \end{aligned} \tag{13}$$

where $0 \leq \theta \leq 2\pi$. Then the Hough accumulation voting space is a three-dimensional space defined by (a, b, r) in which local maxima correspond to the discovered circles in the image.

We apply the CHT algorithm on the edge data of the original scanned grayscale asographic map data that is produced by Sobel operators ([4]):

$$S_x = \begin{bmatrix} -1 & 0 & 1 \\ -2 & 0 & 2 \\ -1 & 0 & 1 \end{bmatrix}, S_y = \begin{bmatrix} -1 & -2 & -1 \\ 0 & 0 & 0 \\ 1 & 2 & 1 \end{bmatrix} \tag{14}$$

After Sobel edge detection, we reduce the high-frequency noise by applying a Gaussian blur filter with kernel size 21×21. This step of the method significantly improves the results from the CHT, since many of the faint stars images and other faint objects are suppressed.

On Fig. 8 are shown the results of the two preliminary steps before CHT is applied on the particular segment of the astrographic map. Fig. 8a shows the raw grayscale data of a square region from map ROB033 / 08. We have all square regions segmented by the réseau segmentation, described in Sec. 3. Fig. 8b shows as positive image the result of the Sobel edge detection. The

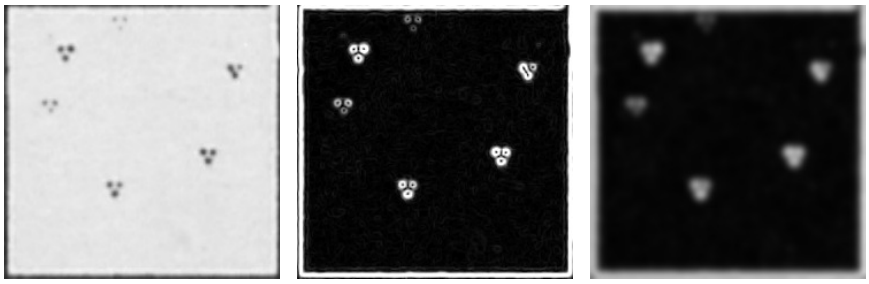

(a) (b) (c)

Fig. 8. (a) A square region of ROB033 / 08; (b) on which we apply the Sobel operators; (c) and after that we reduce the noise with a Gaussian lowpass filter

image contains images of stars that are too faint to extract data from, which are removed by the Gaussian lowpass filtering, the result from which is given on Fig. 8c. The images with the filtered edges are processed by CHT to detect the circular objects in the map.

After the circle detection step of the CHT, we apply a *clustering procedure* that groups the detected circles into segmented asterisms. The clustering procedure is based on the following set of rules.

Rule A. Verify the intensity levels of the detected circles to filter out false candidates that would be otherwise grouped and violate the number of stars images in an asterism.

Rule B. For each two circles c_i and c_j, calculate the Euclidean distance between their centers $d(c_i, c_j)$. If $d(c_i, c_j) \leq d_{th}$, c_i and c_j are labeled as potential members of the same group. The threshold value d_{th} is estimated 12 experimentally. Remove the circles that cannot be grouped according to the distance criterion.

Rule C. Exclude those groups that are result from the Rule B that have more than three members as overlapped asterisms. Overlapped asterisms cannot be used in the flare stars detection algorithm.

Rule D. Verify geometrically that grouped circles form a triangle, using the triangle inequality applied on the resulting sides defined by the centers of the circles.

Rule E. Verify that the triangle formed by the group is close to equilateral by checking the angles formed by its vertices.

Rule F. Check the orientation of the formed triangle. All asterisms in the astrogaphic map have the same orientation.

The result of the clustering algorithm is the set of successfully grouped asterisms with their bounding boxes, and those circles detected by CHT, that violate rules A – F and are discarded.

Fig. 9 shows the segmented asterisms in three square regions in the astrographic map ROB033 / 08. In yellow are marked the images of the stars that are

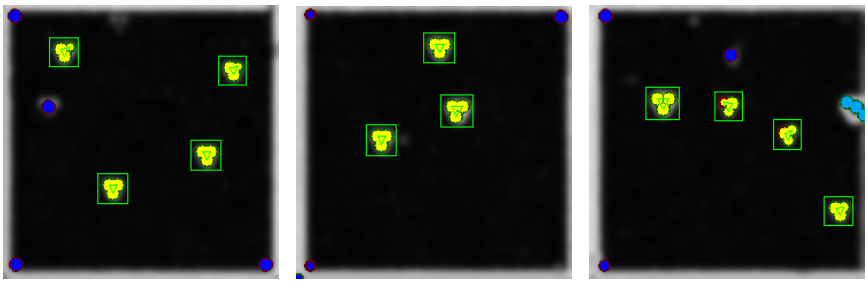

(a) (b) (c)

Fig. 9. Segmented asterisms in yellow in their bounding boxes, in blue detected circles that form a group of less than three members, and in light blue a group that do not form an asterism because Rule B is violated

successfully grouped as asterism. The green frame shows the calculated bounding box of each asterism. In blue are marked circles that are detected by CHT, but they form a group composed by less than three members. In light blue are shown detected circles that violate Rule B, and that is why they are discarded.

5 Implementation and performance

The algorithms described in the in Sec. 3 and Sec. 4 are implemented in C++ programming language using the Qt framework. The implementation is composed by the following main classes and modules:

- CarteDuCiel – the main class of the project that implements the majority of the driver routines;
- OtsuSegmentation – implementation of the Otsu's algorithm;
- ProjectionsCalculator – implements projection profiles histogram analysis;
- DerivativesCalculator – routines that analyze the projection profiles based on discrete derivatives; these algorithms are used mainly to experiment and compare with the presented method in Sec. 3;
- GridLinesDetector – routines that segment the réseau based on the analysis of the projection profiles in the class ProjectionsCalculator;
- ROIAnalyzer – routines that perform the processing of the square regions of the astrographic maps defined by the segmented réseau;
- MinimumSpanningWindows – routines that calculate the bounding boxes of each segmented asterism;
- DBStoreHandler – interface to the database management system that manages a relational database of segmented asterisms; the database is local, based on PostgreSQL and will be used to train and test the convolutional neural network [7].

To verify the computational performance of the asterism segmentation algorithm, we are applying *precision*, *recall* and F_1 score [2]. In our case *true positive*

TP denotes the number of asterism that are correctly recognized, *false negative* FN denotes the number of asterisms that are not detected by the algorithms, and *false positive* FP are the number of objects that are not asterisms, but are recognized as such. The numerical results for the astrographic map ROB033 / 08 are given in Table 1.

Table 1. Computational performance of the asterism segmentation algorithm

TP	FN	FP	Precision	Recall	F_1
752	416	14	0.975	0.644	0.775

We will note that the astrographic maps contain many asterisms that are overlapped or are distorted by the réseau, that explains the number of FN in our experiments. Also, the distorted asterisms cannot serve in the next step of the flare stars detection performed by the convolutional neural network [7].

6 Conclusion

In this paper we describe our method for astographic maps images segmentation. The proposed approach covers two main subtasks: the segmentation of the square coordinate grid called réseau, and the segmentation of the triple stars images, called asterisms. The described algorithms are implemented in C++ programming language with Qt framework.

The réseau segmentation is implemented using the projective profiles of the binarized images. We suppress the high-frequency noise in the profiles using a lowpass filter that allows us to implement a threshold algorithm that extracts the maxima that correspond to the lines of the grid. The segmented réseau is used to partition the map image into 26×26 square regions that are processed separately in the next stage of the method.

The segmentation of the asterisms is implemented using a Circle Hough Transform and a clustering algorithm based on a set of six grouping rules. Our experiments show that the proposed method successfully segments and calculates the bounding boxes of the asterisms that are clearly distinguishable in the map, which are actually data of interest for the recognition of flare stars.

As future work, we are building a dataset of the detected astrisms in the astrographic maps of the plates of the Royal Observatory of Belgium that were included in WFPDB [14]. The data set will be composed by the segmented images of asterisms, defined by their bounding boxes, and metadata defined by the segmented réseau. Also, we will speed up significantly the implemented software by adopting parallel computing for the stage of asterisms segmentation, because each square region of the map can be processed individually.

The resulting dataset of segmented asterisms will be used to train and test our implementation of convolutional neural network for astersms classification flare stars detection in astrographic maps [7].

References

1. Ballard, D.: Generalizing the Hough transform to detect arbitrary shapes. Pattern recognition **13**, 111–122 (1981). https://doi.org/10.1016/0031-3203(81)90009-1
2. Fawcett, T.: An introduction to roc analysis. Pattern recognition letters **27**(8), 861–874 (2006). https://doi.org/10.1016/j.patrec.2005.10.010
3. Fresneau, A., Argyle, R.W., Marino, G., Messina, S.: Potential of astrographic plates for stellar flare detection. The Astronomical Journal **121**(1), 517–524 (January 2001). https://doi.org/10.1002/nav.3800020109
4. Gonzalez, R.C., Woods, R.E.: Digital Image Processing. Pearson, 330 Hudson Street, New York, NY 10013 (2018)
5. Hough, P.V.: Method and means for recognizing complex patterns (12 1962), US Patent 3,069,654
6. Jones, D.: The scientific value of the Carte du Ciel. Astronomy & Geophysics **41**(5), 5.16–5.20 (October 2000). https://doi.org/10.1046/j.1468-4004.2000.41516.x
7. Laskov, L.M., Radev, R.: Implementation of a CNN for asterism classification in Carte du Ciel astrographic maps. In: Zlateva, T., Tuparov, G. (eds.) Computer Science and Education in Computer Science. pp. 102–114. Lecture Notes of the Institute for Computer Sciences, Social Informatics and Telecommunications Engineering, Springer Nature Switzerland (2023). https://doi.org/10.1007/978-3-031-44668-9˙8
8. Laskov, L.M., Tsvetkov, M.: Data extraction form Carte du Ciel tripple images. Serdica Journal of Computing **7**(4), 317–332 (2013)
9. Lehtinen, K., Prusti, T., de Bruijne, J., Lammers, U., Manara, C.F., Ness, J.U., Siddiqui, H., Markkanen, T., Poutanen, M., Muinonen, K.: Digitization and astrometric calibration of Carte du Ciel photographic plates with Gaia DR1. Astronomy & Astrophysics **616**, A185 (2018). https://doi.org/10.1051/0004-6361/201832662
10. Lehtinen, K., Prusti, T., de Bruijne, J., Lammers, U., Manara, C.F., Ness, J.U., Siddiqui, H., Poutanen, M., Muinonen, K., Morrison, O.: Carte du Ciel and Gaia - I. astrometry. Astronomy & Astrophysics **671**(A16), 1–20 (2023). https://doi.org/10.1051/0004-6361/202142929
11. Ortiz-Gil, A., Hiesgen, M., Brosche, P.: A new approach to the reduction of Carte du Ciel plates. Astron. Astrophys. Suppl. Ser. **128**(3), 621–630 (1998). https://doi.org/10.1051/aas:1998168
12. Otsu, N.: A threshold selection method from gray-level histograms. IEEE Transactions on Systems, Man, and Cybernetics **9**(1), 62–66 (1979). https://doi.org/10.1109/TSMC.1979.4310076
13. Tensmeyer, C., Martinez, T.: Historical document image binarization: A review. SN Computer Science **1**(3), 173 (2020). https://doi.org/10.1007/s42979-020-00176-1
14. Tsvetkova, K., Tsvetkov, M., Kalaglarsky, D., Lampens, P., Duval, D.: Analysis of the Uccle Carte Du Ciel catalogue (rob033) present in the WFPDB. Astronomy and Space Science **121**, 177–186 (2007)
15. Urban, S.E.: New reductions of the Astrographic Catalogue: high accuracy, early epoch positions for proper motion studies. International Astronomical Union Colloquium **165**, 493–498 (1997). https://doi.org/10.1017/S025292110004700X
16. Yuen, H., Princen, J., Illingworth, J., Kittler, J.: Comparative study of hough transform methods for circle finding. Image and vision computing **8**(1), 71–77 (1990). https://doi.org/10.1016/0262-8856(90)90059-E